J Neurophysiol 97: 3057–3069, 2007.
First published January 3, 2007; doi:10.1152/jn.00897.2006.

Calibration of Visually Guided Reaching Is Driven by Error-Corrective Learning and Internal Dynamics

Sen Cheng and Philip N. Sabes
Sloan-Swartz Center for Theoretical Neurobiology, W. M. Keck Center for Integrative Neuroscience and Department of Physiology, University of California, San Francisco, California

Submitted 22 August 2006; accepted in final form 16 December 2006

Cheng S, Sabes PN. Calibration of visually guided reaching is driven by error-corrective learning and internal dynamics. *J Neurophysiol* 97: 3057–3069, 2007. First published January 3, 2007; doi:10.1152/jn.00897.2006. The sensorimotor calibration of visually guided reaching changes on a trial-to-trial basis in response to random shifts in the visual feedback of the hand. We show that a simple linear dynamical system is sufficient to model the dynamics of this adaptive process. In this model, an internal variable represents the current state of sensorimotor calibration. Changes in this state are driven by error feedback signals, which consist of the visually perceived reach error, the artificial shift in visual feedback, or both. Subjects correct for ≥20% of the error observed on each movement, despite being unaware of the visual shift. The state of adaptation is also driven by internal dynamics, consisting of a decay back to a baseline state and a "state noise" process. State noise includes any source of variability that directly affects the state of adaptation, such as variability in sensory feedback processing, the computations that drive learning, or the maintenance of the state. This noise is accumulated in the state across trials, creating temporal correlations in the sequence of reach errors. These correlations allow us to distinguish state noise from sensorimotor performance noise, which arises independently on each trial from random fluctuations in the sensorimotor pathway. We show that these two noise sources contribute comparably to the overall magnitude of movement variability. Finally, the dynamics of adaptation measured with random feedback shifts generalizes to the case of constant feedback shifts, allowing for a direct comparison of our results with more traditional blocked-exposure experiments.

INTRODUCTION

Subjects exhibit rapid and robust adaptation in the face of altered feedback in many simple sensorimotor tasks (Held and Gottlieb 1958; Miles and Fuller 1974; Optican and Robinson 1980; Welch 1978). In the study of these forms of plasticity a fundamental question arises: How does sensory feedback drive learning? We address this problem from a psychophysical and modeling perspective using reach adaptation to shifted visual feedback. Traditionally, studies of reach adaptation use a blocked experimental design, where adaptation is quantified by the difference in performance on two blocks of test trials, before and after exposure to shifted feedback (e.g., Hay and Pick 1966; Held and Gottlieb 1958; Welch et al. 1974). This blocked design focuses on only the final effects of adaptation and so it cannot reveal the processes that link sensory feedback in a given trial to the adaptive responses observed in subsequent trials (Cheng and Sabes 2006; Nemenman 2005).

Recently, a number of researchers used analytic techniques from engineering to study the trial-by-trial dynamics of sensorimotor adaptation. These studies found that adaptation occurs rapidly, on the timescale of single trials, when a random shift was added to the visual feedback of the fingertip (Baddeley et al. 2003) or when perturbing forces were introduced during reaching (Donchin et al. 2003; Scheidt et al. 2001; Thoroughman and Shadmehr 2000). However, subjects in these studies were aware of the experimental manipulations, either as a result of the explicit instructions regarding the visual shift or of the presence of noticeable force perturbations. Therefore learning likely reflected a combination of automatic sensorimotor processes and strategic cognitive approaches to the task. These two forms of learning obey very different underlying learning rules. For example, when subjects are aware of a shift in visual feedback, they are able to learn much more complex shift patterns then when they are not aware of the shift (Bedford 1993). The goal of the present study was to quantify the trial-by-trial dynamics of the automatic processes of sensorimotor adaptation—that is, the processes that are presumably responsible for the ongoing maintenance of sensorimotor calibration. We therefore study the adaptive responses of naïve subjects to surreptitious shifts in visual feedback.

As in previous studies, we model the trial-by-trial dynamics of learning as a linear dynamical system (LDS). However, we make use of the analytic methods described in Cheng and Sabes (2006), allowing us to explore two issues that were not dealt with in earlier studies. First, instead of using least-squares regression to perform model fits, we take a more general maximum-likelihood approach. This allows us to build explicit models of the sources of variability in task performance and to fit these models to experimental data. As we will show, such variability plays an important role in the dynamics of adaptation. Second, we consider multiple potential error-feedback signals and attempt to determine which of these signals drive learning.

This study focused on the sequence of reach errors induced by a sequence of visual feedback shifts. We view these errors as a reflection of the underlying state of reach adaptation. By using a random, time-varying sequence of feedback shifts, we obtained a statistically rich sequence of reach errors that was modeled as an LDS (Cheng and Sabes 2006). We found that this class of models is sufficient to describe the adaptation dynamics: the LDS model captures both the changes in the

Address for reprint requests and other correspondence: P. N. Sabes, Department of Physiology, University of California, San Francisco, CA 94143-0444 (E-mail: sabes@phy.ucsf.edu).

The costs of publication of this article were defrayed in part by the payment of page charges. The article must therefore be hereby marked "*advertisement*" in accordance with 18 U.S.C. Section 1734 solely to indicate this fact.

mean reach endpoint and the temporal correlations between these errors and the visual shift.

We draw several conclusions from the resulting model of adaptation dynamics. First, significant adaptation to visual feedback shifts occurs on single trials. Second, we explicitly measure the internal dynamics of adaptation and show that the state of adaptation decays over time. Third, a significant source of movement variability is internal state noise that directly affects the state of adaptation and thus accumulates across trials. This form of variability only indirectly affects the performance on a particular trial. We show that the state noise accounts for at least a quarter of the overall movement variability, thus offering a very different perspective on the sources of movement variability.

Finally, to relate these results to previous research using the blocked experimental design, we used the model derived from stochastic feedback trials to predict the sequence of reach errors induced by blockwise-constant feedback shifts. We find that the adaptation dynamics generalizes across feedback shift conditions. We conclude that the dynamics of adaptation are not specific to the sequence of feedback shifts and that the LDS model can provide insight into the general mechanisms of reach calibration.

METHODS

Experimental setup and data collection

This study was approved by the University of California, San Francisco Committee on Human Research, and subjects gave informed consent. Ten right-handed subjects (four male, six female, ages 18–28 yr) with no known neurological history and normal or corrected-to-normal vision participated in this study. Subjects were naïve to the purpose of the experiment and were paid for their participation.

The experiment consisted of trials in which subjects reached toward visual targets with their right arm with virtual visual feedback (Fig. 1*A*). Throughout each session, the right arm remained on or just above a horizontal table with direct view of the arm (and the rest of the body) occluded by a mirror and a drape. The right wrist was fixed with a brace in the neutral, pronate position and the index finger was extended and fixed with a splint. An infrared light-emitting diode was attached to the tip of the index finger and its position was recorded at 200 Hz with an Optotrak infrared tracking system (Northern Digital, Waterloo, Canada). Because the subject's hand was essentially restricted to a two-dimensional workspace, we analyzed only two components of the recorded positions: the positive *x*-axis points right and the positive *y*-axis points sagittally away from the subject.

Target positions and virtual visual feedback of the fingertip location (when available) were generated by a liquid crystal display projector (1,024 × 768 pixels, 75 Hz) and viewed in the mirror by a rear-projection screen, placed so that projected images appeared to lie in the plane of the table, at the vertical level of the fingertip. In some trials, the visual feedback was shifted relative to the true location of the fingertip, as subsequently described. All subjects reported being unaware of any such feedback manipulation in a postexperiment questionnaire.

Task design

The purpose of this experiment was, first, to identify the adaptation dynamics in response to stochastic feedback shifts (STOCH-P) and, second, to compare the dynamics with those observed in trial blocks with constant feedback shift (CONST-P), the traditional paradigm for inducing adaptation.

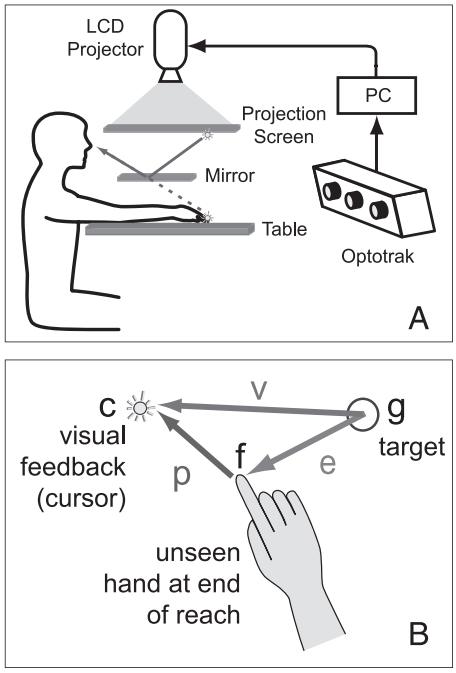

FIG. 1. *A*: virtual feedback setup. *B*: definition of reach and feedback variables: f, location of unseen fingertip location at end of reach; c, location of visual feedback (cursor); g, target location; e, true reach error; v, visually perceived reach error; p, artificial feedback shift (perturbation).

An experimental session consisted of four repetitions of the following sequence of trial blocks: 25 transition trials (see following text), 35 CONST-P trials, 10 transition trials, and 50 STOCH-P trials. Within each CONST-P trial block the feedback shift was constant, but the shift varied between the four CONST-P block. The four shifts were a random ordering of the four vectors with ±3 cm along both the *x*- and *y*-axes. Transition trials with either unshifted visual feedback or no visual feedback were inserted to minimize the possibility that subjects became aware of manipulations in the visual feedback. Each CONST-P trial block was preceded by 15 trials with unshifted feedback and then 10 trials without visual feedback. When a CONST-P block followed a STOCH-P block, the shift was ramped down to zero over the first five of these transition trials. Each CONST-P block was also followed by 10 trials without visual feedback. In total, each session consisted of 480 trials, with 200 STOCH-P trials and 140 CONST-P trials. An example session is shown in Fig. 2.

STOCHASTIC FEEDBACK-SHIFT SEQUENCE. We expect that reach adaptation will be driven by either the artificial shifts in visual feedback, the resulting visually perceived reach errors, or a combination of both. In other words, these signals will be the "inputs" that drive changes in the state of adaptation. To identify the trial-by-trial dynamics of adaptation, these inputs have to be "rich" enough to excite all the modes of the dynamics (e.g., Ljung 1999). Feedback shifts that follow a white-noise sequence would be ideal, especially because they decorrelate the input sequence and the state (Cheng and Sabes 2006). However, in pilot experiments subjects often became aware of these shifts, creating the possibility of explicit cognitive strategies. Therefore we used a modified random-walk sequence of visual shifts for this study.

From one trial to the next, the shift in visual feedback (*p*; see Fig. 1*B*) changed incrementally by one of the following (*x*, *y*) vectors, selected with equal probability: (0, 0), (0, *sy*), (*sx*, 0), or (*sx*, *sy*)/$\sqrt{2}$, where $|sx| = |sy| = 5.2$ mm, and initial signs of *sx* and *sy* were assigned randomly at the beginning of each block. The maximum magnitude of the feedback shift in either dimension was limited to ±3 cm. If the selected increment would have caused the *x* or *y* component

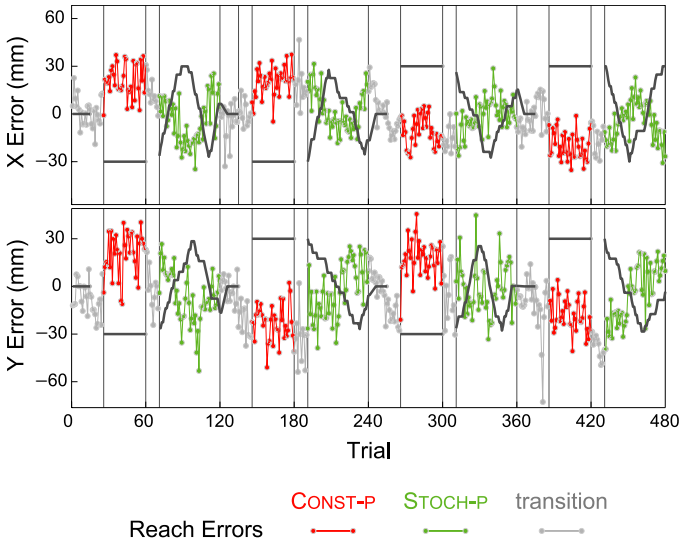

FIG. 2. Example trial sequence. Visual feedback shifts (*black traces*) and reach errors (see key at *bottom*) along the *x*-axis (*top*) and *y*-axis (*bottom*) are shown. Gray vertical bars mark boundaries between blocks of trial types: STOCH-P: stochastically shifted feedback; CONST-P: constant feedback shift; transition: trials include reaches without visual feedback to prevent subjects from noticing onset of constant shift blocks and ramping down of shift after a STOCH-P block.

of the feedback shift to exceed this range, then the sign of *sx* or *sy*, respectively, was reversed (reflecting boundaries). In each trial block, the feedback shift in the first trial was the value used in the last preceding trial with feedback. Example random-walk sequences are shown in the STOCH-P blocks of Fig. 2.

REACH TRIALS. Every trial in the experiment consisted of reaching to a visual target. At the beginning of each of these trials, subjects were guided to a start position without visual feedback about either the start location or their hand ("arrow field" technique; Sober and Sabes 2005). Specifically, an array of 3 × 3 identical arrows appeared in a randomized position of the workspace. The arrows corresponded to the vector from the current finger position to the start position, with a maximal length of 9 cm. Subjects were instructed to move their finger in the direction indicated by the orientation of the arrows until the arrows disappear, which occurred when the fingertip was within 5 mm of the unmarked start position. The start position was the same for all trials and was located a few centimeters in front of the subject, roughly along the midline.

Subjects were required to hold the start position for a random delay (0.5–1 s) until the reach target appeared (an open green circle, radius 6 mm). The target location g_t was drawn randomly from a uniform distribution over a 4-cm square centered 26 cm distally from the start location. The appearance of the target together with an audible tone constituted the go signal for initiating the reach. Subjects were instructed to make a single quick and smooth movement toward the target. The trial terminated when the velocity of the finger fell to <2 mm/s.

To minimize variation in movement speed across trials, a loose timing constraint was used. The movement duration was defined as the length of the time interval between when the finger first moved >1 cm from the start location and when the tangential velocity of the finger first fell to <15% of its peak value at the end of the movement. These landmarks were chosen to exclude effects of variable reaction time and movement corrections at the end of the reach. A tone was sounded if reaches were too slow (movement duration >500 ms) or too fast (movement duration <300 ms). Subjects generally had no difficulty meeting these criteria.

Subjects received "velocity-dependent terminal feedback." Visual feedback of the finger tip position appeared only near the end of the movement, when the tangential finger velocity fell to <15% of the peak value and feedback continued until the end of the trial. This arrangement satisfies two constraints. The feedback appears sufficiently late in the movement so that we are able to assess the endpoint of the initial reach before visual feedback is able to drive corrective changes. The endpoint is thus taken as a measure of the state of the reach adaptation. However, the brief period of visual feedback while the hand is still moving provides a richer feedback signal for learning than would static feedback after the completion of the movement. Feedback was in the form of a white disk, 3-mm radius, located at the fingertip or displaced by the feedback shift p_t. Finally, subjects were instructed to correct any reach errors after completing the first reach and trials terminated when the finger remained stationary within the target circle for 500 ms.

In some transition trials subjects received no visual feedback of their reaching arm during any part of the trial. These trials were identical to those with visual feedback, except that the target was marked by a filled green circle with radius 6 mm, providing a cue of the feedback type before reach initiation. Before data collection subjects were given sufficient practice trials to ensure that all task constraints were met.

Data analysis and a model for the dynamics of adaptation

Velocities were determined by first-order numerical differentiation of the positional data after smoothing with a 5-Hz low-pass Butterworth filter. The reach endpoint f_t on trial t was defined as the finger position when the tangential velocity first fell to <5% of its maximum value on that trial. Typical velocity profiles were unimodal bell-shaped curves (cf. Atkeson and Hollerbach 1985), corresponding to the primary reaching movement, followed by one or more smaller peaks attributed to corrective movements. In a few trials the velocity fell to <5% criterion only after the second velocity peak. In these cases visual inspection usually indicated a clear endpoint for the primary reach (velocity dip and curvature peak); in the rare cases, however, where an endpoint could not be identified confidently the trial was discarded. The reach error e_t is defined as the difference between the target position g_t and the reach endpoint f_t (Fig. 1*B*): $e_t \equiv f_t - g_t$.

We use a linear dynamical systems (LDS) model to describe the adaptation dynamics (Cheng and Sabes 2006; Donchin et al. 2003; Scheidt et al. 2001). The output of the system y_t is a noisy readout of the internal state of the sensorimotor map x_t. Here we define y_t to be the reach error e_t. This means that the internal state of the system is defined as the mean reach error one would observe across trials if adaptation could be frozen in time. Given the limited set of reach vectors used in this experiment, the state can be described with a single two-dimensional variable. Formally we write

$$\text{LDS Output: } y_t = x_t + r_t \tag{1a}$$

where r_t is the sensorimotor noise, or output noise, in trial t, assumed to be an independent zero-mean, Gaussian random variable with a covariance matrix R, i.e., $r_t \sim N(0, R)$. We model adaptation as the trial-by-trial change in the state arising from sensory feedback on the preceding trial. Formally

$$\text{LDS Update: } x_{t+1} = Ax_t + Bu_t + q_t \tag{1b}$$

where u_t represents the sensory feedback variables (inputs) driving adaptation and q_t is additive noise in the state variable, assumed to be independent, zero-mean, Gaussian with covariance Q, i.e., $q_t \sim N(0, Q)$. The term Bu_t represents error corrective learning, Ax_t represents the decay of the state of adaptation back to baseline, and q_t represents variability in these two processes. Because the spatial variables are all two-dimensional vectors, the parameters of the LDS

model, A, B, Q, and R, are 2×2 matrices. There are no direct "feedthrough" inputs affecting y_t because terminal visual feedback prevents on-line visual correction and the ongoing reaches were not otherwise externally perturbed.

An important variable in the LDS model of *Eq. 1* is the feedback signal that drives adaptation u_t. Our experimental design makes the selection of candidate signals easier because visual feedback is given only near the end of the movement, representing only the location of the index fingertip (Fig. 1*B*). Under these conditions, there are two likely candidates for the input signal: the visually perceived error v_t, defined as the difference between the position of the visual feedback at the reach endpoint and the target position, $v_t \equiv c_t - g_t$, and the artificial feedback shift p_t (Fig. 1*B*). We also consider the reach error e_t as a potential input signal. Note that the three error signals are linearly related: $e_t = v_t - p_t$. Therefore any model that includes two of these variables effectively includes the third one as well.

Given a sequence of inputs u_t and outputs y_t, the maximum-likelihood estimates of the model parameters A, B, Q, and R are determined using an expectation-maximization (EM) algorithm (Cheng and Sabes 2006; Ghahramani and Hinton 1996; Shumway and Stoffer 1982) (Matlab routines for performing this analysis are freely available at http://keck.ucsf.edu/~sabes/software/). The algorithm takes into account that data were collected in separate blocks by resetting the state to an initial Gaussian distribution (with the necessary additional model parameters) at the beginning of each block. The EM algorithm is guaranteed only to converge to a local maximum of the log likelihood. In fact, however, we find that the parameter estimates were robust to running the estimation algorithm with different sets of initial values, suggesting that no local minima exist close to the identified parameter estimates.

Model comparisons and goodness of fit

The EM algorithm will find a maximum-likelihood model for any input and output sequence. Therefore it is important to be able to assess model performance. We begin with model selection, asking whether particular model parameters—in this case input signals—provide significant explanatory power. We then describe two approaches to quantifying whether the best-fit model is sufficient to account for important statistical features of the input–output sequences. These analyses are described in detail below.

LIKELIHOOD RATIO TEST FOR MODEL SELECTION. To determine whether the inclusion of a particular input variable or other parameter provides significant explanatory power we use the generic likelihood ratio test (LRT) for maximum-likelihood estimation (Stuart and Ord 1987). Consider a model class M_1 with d_1 free parameters and a second model class M_0, with a subset of free parameters, $d_0 < d_1$. For example, M_1 could be the model with a particular two-dimensional input variable u_t and M_0 could be the null model with no input variables. M_0 has four fewer free parameters because it has no input weighting matrix B. Given each model class, we can find the maximum-likelihood model parameters and the values of likelihood they achieve, L_i for model M_i. The inclusion of additional model parameters will always result in a better fit to the data, i.e., $L_1 > L_0$. However, under the assumption that the data come from a model in M_0, the distribution of gains in log likelihood resulting only from overfitting is known in the limit of large data sets

$$2 \log \frac{L_1}{L_0} \sim \chi^2_{d_1 - d_0} \tag{2}$$

Using this distribution, the LRT either accepts or rejects the additional parameters.

PREDICTING THE STATISTICS OF THE REACH ERRORS. The most direct approach to assessing model sufficiency would be to compare the empirical output sequence y_t with the outputs predicted from the model and the input sequence. However, the outputs depend heavily on the specific sequence of state noise terms q_t, which are not directly observable. Instead, we determine how well models are able to predict the statistics of the sequence of reach errors and the relationship to the sequence of visual shifts.

The sequence of reach errors is characterized by two measures: the variance σ_e^2 and the autocorrelation $\rho_e(\tau)$, which is a function of the time lag τ at which the autocorrelation is measured. Similarly, the statistical relationship between the reach error and the visual shift vector is characterized by two measures: the covariance σ_{ep} and the cross-correlation function $\rho_{ep}(\tau)$. These measures are defined as follows

$$\sigma_e^2 = \frac{1}{T} \sum_t (e_t - \bar{e})^{\mathrm{T}} (e_t - \bar{e}) \tag{3a}$$

$$\rho_e(\Delta t) = \frac{1}{T\sigma_e^2} \sum_t (e_t - \bar{e})^{\mathrm{T}} (e_{t-\Delta t} - \bar{e}) \tag{3b}$$

$$\sigma_{ep} = \frac{1}{T} \sum_t (e_t - \bar{e})^{\mathrm{T}} (p_t - \bar{p}) \tag{3c}$$

$$\rho_{ep}(\Delta t) = \frac{1}{T\sigma_e\sigma_p} \sum_t (e_t - \bar{e})^{\mathrm{T}} (p_{t-\Delta\tau} - \bar{p}) \tag{3d}$$

where T is the total number of trials, $\bar{a}$ represents the mean value of a vector a across trials, and $a^{\mathrm{T}}b$ represents the inner product of the vectors a and b.

The statistics defined earlier provide a summary of the adaptive response of the reach endpoint to the shifted visual feedback. These statistics were not used explicitly when performing the maximum-likelihood model fitting. Thus if the model is able to accurately predict these statistics, then it is sufficient to capture the key elements of the response. The model predictions for these statistics are obtained using a Monte Carlo approach. Given the LDS model parameters and actual sequence of visual shifts experienced by the subject in a given trial block, we simulate a sequence of state and output variables using *Eq. 1*, with state and output noise terms generated independently for each simulated trial. For each subject, we compute the desired statistics from 100 combined runs of these Monte Carlo simulations and compare the values to those obtained from the empirical data.

ONE-STEP-AHEAD PREDICTION AND THE PORTMANTEAU TEST. Our second approach to assessing sufficiency is to test whether an LDS model is demonstrably insufficient to account for the dynamics of the sequence of reach errors. We start with the one-step-ahead predictor $\hat{y}_t$, which is the expected value of y_t given a model and all the inputs and outputs up to trial $t - 1$. The $\hat{y}_t$ values are obtained from the Kalman filter using the estimated model parameters (Anderson and Moore 1979; Shumway and Stoffer 1982). However, if the LDS model being used to predict the same data set on which it was fit, a cross-validation procedure is used: the one-step-ahead predictions $\hat{y}_t$ for each block of 25 trials are computed using a model fit to the data set with that block excluded.

If the model satisfactorily captures the adaptation dynamics, then the one-step-ahead prediction residuals $y_t - \hat{y}_t$ should be free of temporal correlations, i.e., the residuals should be a white-noise sequence. We can compare this null hypothesis to the alternative (significant residual correlations exist) using a portmanteau test for

serial autocorrelations (Hosking 1980). This test is based on the autocorrelations of the prediction errors at a lag of τ trials

$$J_\tau = \langle (y_{t+\tau} - \hat{y}_{t+\tau})(y_t - \hat{y}_t)^{\mathrm{T}} \quad (4)$$

The mth portmanteau statistic combines the autocorrelation at lags up to m trials

$$P_m = T^2 \sum_{\tau=1}^{m} \frac{1}{\mathrm{T} - \tau} \mathrm{tr}\,(J_\tau^{\mathrm{T}} J_0^{-1} J_\tau J_0^{-1}) \quad (5)$$

Under the null hypothesis, the model captures the statistical structure of the output sequence, and so the J_τ and (thus) the P_m should be smaller than if the model were not sufficient. In the case of no inputs to the system and in the limit of large T, P_m is χ^2 distributed under the null hypothesis (Hosking 1980). When there are inputs to the system, as is typically the case here, the theoretical distribution of the portmanteau statistic is unknown. Therefore we use Monte Carlo simulation to estimate the distribution of the portmanteau statistic under the LDS model, given the known sequence of feedback shifts p_t. First, we simulate 1,000 artificial data sets, as described in the previous section. For each of these artificial data sets we compute the portmanteau statistic P_m. This yields an empirical distribution of 1,000 samples for P_m under the assumption of the LDS model. If the portmanteau statistic calculated from the actual data is larger than the 95th percentile of this distribution, then we reject the null hypothesis and say that the model is not sufficient to account for the sequence of reach errors.

Although the portmanteau test can be used for any maximum lag m, the statistical power of the test decreases with the lag (Davies and Newbold 1979). On the other hand, larger lags need to be included in the portmanteau statistic to test for long-range residual autocorrelations. As a compromise, we will present the portmanteau statistic for maximum lags m up to eight trials, although no substantial differences were noted for maximum lags $\leq$20 trials.

RESULTS

We are primarily concerned with the trial-by-trial sequence of reach errors, which reflects the changing state of reach adaptation. A sequence from a typical session is shown in Fig. 2. Two salient features of these plots highlight the key elements of the dynamics of adaptation. First, over the course of a block, the reach errors are strongly influenced by the direction of the visual feedback shift: the error appears to roughly track the inverse of the shift. This is the general pattern that is expected when subjects adapt to the shifted feedback. Second, there is considerable variability in reach error from one trial to the next trial, even when there is no time-varying feedback shift.

The goal of this work is to quantify and characterize how such error sequences arise from a combination of error-corrective learning processes and the various sources of variability, including a stochastic component of the internal dynamics of adaptation. In the rest of this paper we use the LDS model of adaptation to accomplish this goal.

Error-corrective learning

We begin by determining which feedback signals, if any, drive error-corrective learning. In terms of the LDS model, this means identifying the inputs that lead to a significantly better fit to the data. The three candidate inputs signals each have a corresponding LDS update (learning) equation

$$\begin{aligned} M_v&: x_{t+1} = Ax_t + Bv_t + q_t \\ M_p&: x_{t+1} = Ax_t + Bp_t + q_t \\ M_e&: x_{t+1} = Ax_t + Be_t + q_t \end{aligned} \quad (6)$$

that represent three classes of LDS models. Two additional model classes are also considered: the null model class

$$M_\varnothing: x_{t+1} = Ax_t + q_t \quad (7)$$

which has no error feedback, and the M_{vp} model class, in which both v_t and p_t contribute to reach adaptation. Because v_t, p_t, and e_t are linearly related, M_{vp} is equivalent to any model that includes at least two of the three input signals. Together, these five model classes form the hierarchy shown in Fig. 3.

We use the likelihood ratio test (LRT) to compare model pairs that differ by the inclusion of a single variable (arrows in the hierarchy of Fig. 3). For each subject, each model class was fit to the sequence of 200 reach errors from the four STOCH-P trial blocks. Both the visually perceived error v_t and the feedback shift p_t significantly improved the fit over the null model for every subject. In contrast, including the reach error e_t did not significantly improve the model for any subjects. These results indicate that the trial-by-trial changes in reach error are not simply the result of a random walk. Rather, we observe an error-corrective adaptation process driven by either the visually perceived error, the feedback shift, or a combination of both.

The relative contributions of these two feedback signals could, in principle, be quantified with the LDS approach. However, there is not sufficient statistical power to accomplish this when there is a strong correlation across trials between the two signals. In our case, the visually perceived error and the feedback shift are related by the expression $v_t = e_t + p_t$, and so we expect them to be correlated. Indeed, across subjects the mean ($\pm$SD) correlation coefficient between v_t and p_t in the STOCH-P trial blocks is 0.35 $\pm$ 0.12. It is thus not surprising that, although both the M_v and M_p single-input models are significant, the two-input model M_{vp} does not yield a significant improvement over either. The same qualitative results are obtained when the model selection procedure is applied to artificial data generated with the best-fit M_v or M_p model,

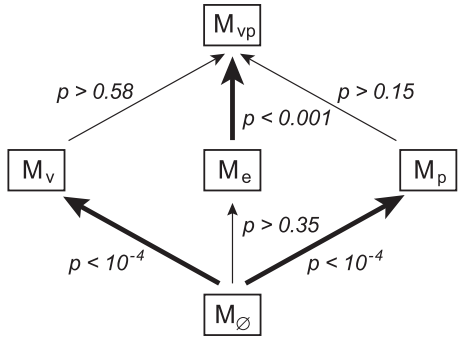

FIG. 3. Hierarchical model selection. Arrows represent comparisons between nested model classes (boxes) made with the likelihood ratio test (LRT) on STOCH-P data. Each test had 4 degrees of freedom, corresponding to 2 $\times$ 2 matrix parameters. P values for the LRT, shown next to the appropriate arrow, apply across all 10 subjects and were highly consistent. Thick lines represent comparisons for which the additional input variable resulted in a significant improvement.

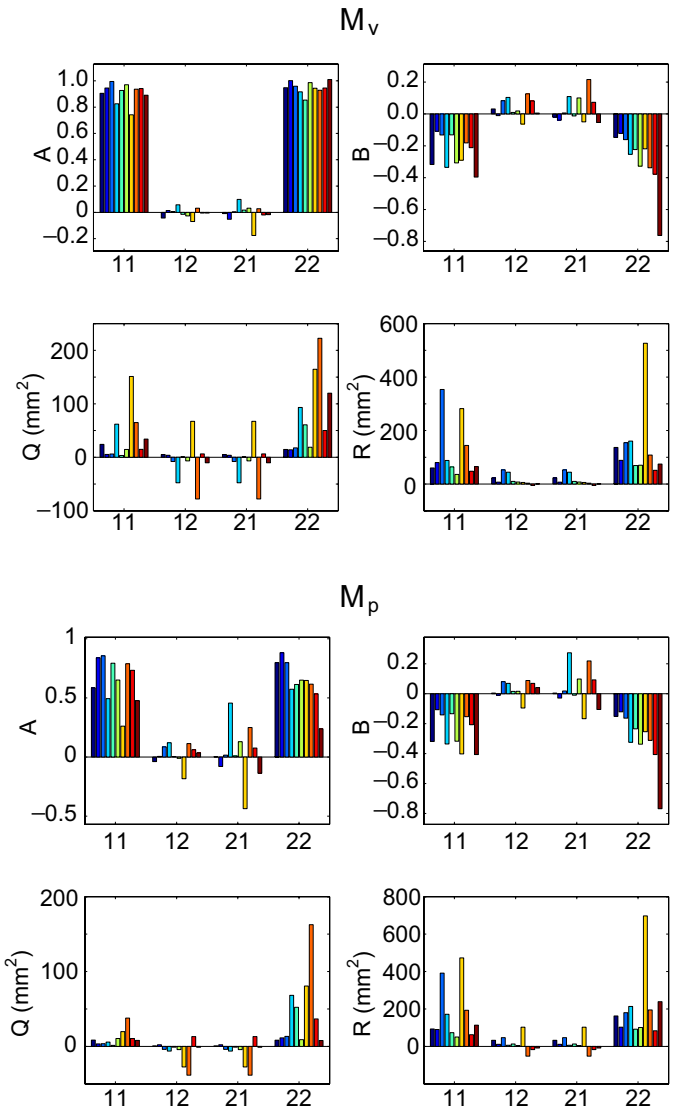

FIG. 4. Maximum-likelihood linear dynamical system (LDS) model parameters. Best-fit parameters for the M_v and M_p models. Each panel represents the values of a 2 × 2-matrix parameter (see labels on ordinate axes), with values for all subjects clustered by the matrix components. Bar colors correspond to subjects ($n = 10$).

underscoring the lack of power to quantify the relative roles of the two feedback signals. Thus in the remainder of the paper we will analyze both the M_v and M_p model classes.

Model parameters

We next consider the maximum-likelihood parameter values for the M_v and M_p model classes (Fig. 4). We will show that the learning rates are quite large, with subjects correcting for about one third of the error feedback after each trial. We will also show that the parameters governing state decay ("forgetting"), state noise, and output noise suggest an important role for each of these processes. Finally, we will show that, although the values for these latter parameters differ between the M_v and M_p model fits, the two model classes are nearly equivalent from the perspective of these data sets.

The best-fit values of the learning parameter B agree quite well between the two model classes (Fig. 4). To interpret these 2 × 2 matrices, we consider the first (second) eigenvalues of B, which represent the maximum (minimum) fraction of the error feedback that is corrected for, depending on the direction of the error vector. The mean and SD of the eigenvalues of B (and the other model parameters) are shown in Table 1. They represent a per-trial correction of the respective error signals (v or p) in the range of 20–50%, across subjects, a rapid pace of learning.

The most pronounced difference between the two model fits is in the value of the "decay" parameter A. The values of A are larger for the M_v model than for the M_p model and there is an appreciably greater consistency across subjects for the M_v model. The first (second) eigenvalues of A represent the maximum (minimum) fraction of the state x_t that has not decayed back to the mean by the next trial, ignoring the inputs u. A value of 1 means no state decay (no forgetting) and a value of 0 means a complete reset of the state after each trial (complete forgetting). For the M_v model, the maximum eigenvalue of A is 0.97 on average, corresponding to a state-decay half-life of 23 trials (Table 1). For the M_p model, the eigenvalues are smaller, with a half-life for the first eigenvector of just three trials.

The parameters Q and R represent the state and output noise, respectively. The best-fit parameter values differ across the two model classes (Fig. 4). However, in both cases the magnitude of the state noise is comparable to that of the output noise. For example, in the M_v model fit, the SD of the state noise along its most variable axis (first eigenvalue) is 8.7 mm, compared with 12.3 mm for the output noise (Table 1). We will return to this comparison later.

Last, we analyze the differences between the M_v and M_p model fits. It might seem odd that the models agree so closely on the learning parameter B, which is applied to different input signals in the two models, whereas they disagree on the state decay parameter A. Nonetheless, these differences are expected given the relationship between the visually perceived error v_t and the feedback shift p_t. To show this we rewrite the state update equations for the two models (*Eq. 6*) using the LDS output (*Eq. 1a*) and the fact that e_t is the LDS output

$$\begin{aligned} M_v\colon x_{t+1} &= A_v x_t + B_v v_t + q_t \\ M_p\colon x_{t+1} &= A_p x_t + B_p p_t + q_t \\ &= A_p x_t + B_p(v_t - e_t) + q_t \\ &= (A_p - B_p)x_t + B_p v_t - B_p r_t + q_t. \end{aligned} \tag{8}$$

where subscripts have been added to the parameter variables for clarity. When the noise term $B_p r_t$ is relatively small, the two models are essentially the same if the two equalities $B_v = B_p$ and $A_v = A_p - B_p$ hold. Even if $B_p r_t$ is not small, however, that term contributes only to the effective state noise and so these

TABLE 1. *Mean (±SD) eigenvalues for the LDS model parameters*

Parameter	M_v	M_p
A	[0.97 0.89] ± [0.03 0.09]	[0.77 0.52] ± [0.13 0.23]
B	[−0.36 −0.18] ± [0.18 0.10]	[−0.38 −0.18] ± [0.18 0.10]
$\sqrt{Q}$	[8.7 4.2] ± [4.4 2.4]	[6.2 2.5] ± [3.4 1.18]
$\sqrt{R}$	[12.3 9.1] ± [5.1 3.2]	[14.6 11.0] ± [5.5 4.1]

Eigenvalues for each 2 × 2 matrix parameter were sorted in descending order and then averaged across subjects. For Q and R, the square root of the eigenvalues was used, and so the parameters represent SDs whose units are in millimeters. A and B are dimensionless.

equalities should hold whenever the M_v and M_p models are fit to the same data set. Indeed, the best-fit values of B for the two model classes are nearly identical (Fig. 4 and Table 1) and across subjects the mean (±SD) value of the expression $A_v - (A_p - B_p)$ is

$$\begin{bmatrix} 0.01 & 0.00 \\ 0.00 & 0.01 \end{bmatrix} \pm \begin{bmatrix} 0.03 & 0.04 \\ 0.01 & 0.01 \end{bmatrix}$$

This analysis shows that the M_v and M_p model classes are essentially equivalent, formally differing only in the structure of the noise terms. Because in the following we focus on these noise terms, we will continue to present results for both model classes, in that they represent endpoints in the continuum of models in which both signals contribute with varying strengths.

Model sufficiency

In the two previous sections, we showed that the visually perceived reach error and/or the visual feedback shift drive a large and significant adaptive response. Here we ask whether our LDS models of that response are sufficient, that is, whether they do a "good enough job" of explaining the trial-by-trial sequence of reach errors.

SAMPLE DATA. Figure 5 shows the sequence of reach errors in the STOCH-P trial blocks for a single subject. In addition, this figure shows one-step-ahead model predictions for three different models, i.e., the predicted reach errors for each trial given the actual inputs and outputs up to the previous trial. The one-step-ahead predictions of the best-fit M_v and M_p models (Fig. 5, *red* and *blue traces*, respectively) largely overlap each other, as expected. These predictions appear to track the errors well, capturing the general trends in the data. However, two other features of these traces should be noted. First, although according to the LRT the M_v and M_p models fit the data significantly better than the null model $M_\varnothing$ (*black trace*), the difference in the one-step-ahead predictions is rather small. This is explained by the fact that the predictor is using all inputs and outputs up to a given trial to predict the output on the next trial. Second, all three models leave a large residual of unpredicted reach error in this sample data set.

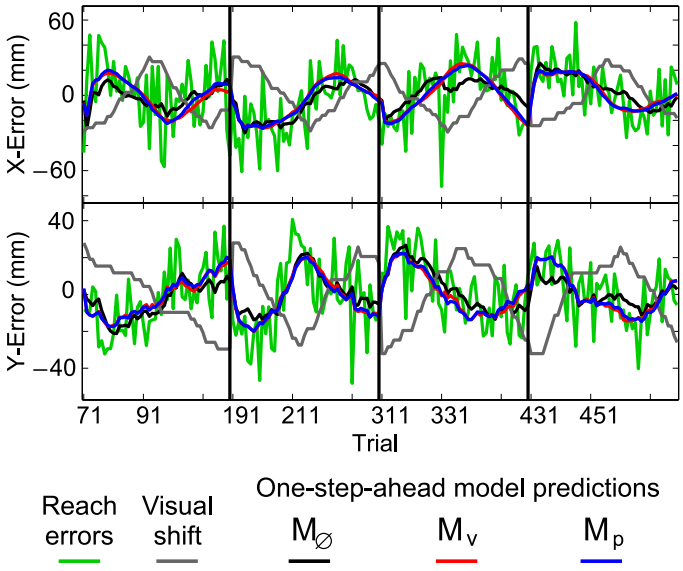

FIG. 5. Sample model predictions. Reach errors and one-step-ahead model predictions for one subject in the STOCH-P trial blocks.

In the remainder of this section we present two approaches to assessing model sufficiency, one addressing the shortcomings of the one-step-ahead predictor and one aimed at the prediction residuals. First we determine how well the models predict the statistical relationship between the reach error and the visual shift. Unlike the one-step-ahead predictor, these predictions are made without access to the real sequence of reach errors, making them a much more stringent test of model sufficiency. Second, we examine the one-step-ahead residuals to determine whether they are as good as can be expected, given the levels of state and output noise, or whether there is still some "signal" to be accounted for.

PREDICTING REACH ERROR STATISTICS. Our first test of model sufficiency is how well a model predicts the statistical structure of the adaptive response to shifted feedback. As described in METHODS, we chose four statistical measures: the variance and autocorrelation of the reach errors and the covariance and cross-correlation between the reach errors and feedback shifts (*Eq. 3*). For each subject, we computed these measures from the empirical sequence of reach errors in the STOCH-P trial blocks. We also computed the measures from 100 combined Monte Carlo simulations of that sequence, generated from the best-fit LDS model and the true sequence of visual feedback shifts (see METHODS).

We first observe that the M_v and M_p models provide a nearly perfect account of the reach variance and autocorrelation (Fig. 6, *A* and *B*). However, the null model performs just as well by these measures. This result shows that the state decay A, state noise Q, and output noise R parameters of the LDS are sufficient to account for the second-order statistics of the reach errors. Furthermore, it shows that the maximum-likelihood–fitting procedure implicitly fits these quantities.

Next we consider the relationship between the reach errors and the sequence of visual feedback shifts. For all subjects, there is a large negative covariance between these variables (Fig. 6*C*), as expected when subjects adapt their reach error to the visual shift. Predicted covariances under the best-fit M_v and M_p models are nearly identical to each other. Although there is a slight downward bias (weaker correlation) in the model predictions, discussed later in greater detail, the predicted and empirical values are strongly correlated across subjects. In contrast, the null model predicts essentially no covariance between the reach error and visual shift. The M_v and M_p model models also provide an excellent prediction of the cross-correlation function between the sequences of reach errors and visual shifts (Fig. 6*D*).

The close agreement between the empirical and predicted error-shift cross-correlation functions raises the question of how sensitive a measure this is. We want to be sure that the predictions depend on the details of the model and are not, for example, dominated by the sequence of visual shifts. Therefore we performed a sensitivity analysis to quantify how the predicted cross-correlation function depends on the model parameters. We generated Monte Carlo simulations with individual parameters altered from their actual best-fit values. The predicted cross-correlations were found to be sensitive to all four parameters and even fairly small parameter changes can produce large discrepancies between the data and model predictions (Fig. 6*E*, results for only M_v are shown).

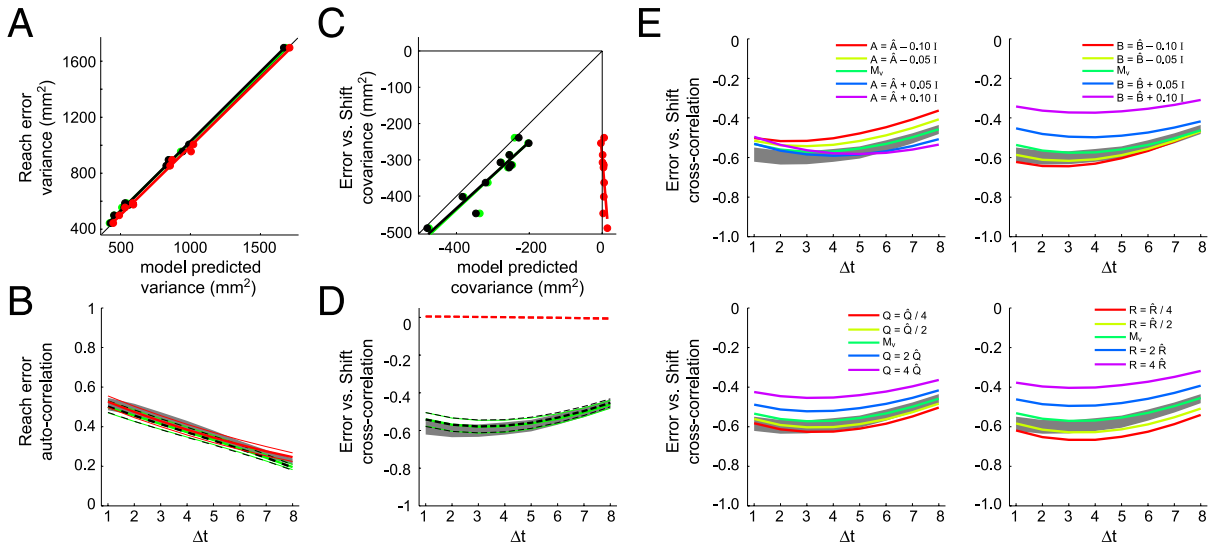

FIG. 6. LDS model is sufficient to predict the statistical structure of the adaptive response to shifted feedback. *A*: comparison of empirical reach error variance σ_e^2 and the predicted variance under the best-fit M_v (black), M_p (green), and $M_\varnothing$ (red) models. Data points represent values for a single subject (symbols overlap); thick lines represent a linear regression of empirical data on prediction ($P < 0.05$). *B*: reach error autocorrelation function $\rho_e(\Delta t)$ for time lags $\Delta t = 1–8$ trials. Dark gray band represents mean ± SE across subjects. Model predictions are shown in 3 lines representing mean ± SE across subjects: M_v, green; M_p, black; $M_\varnothing$, red. *C*: comparison of empirical values and model predictions of the covariance σ_{ep} between reach errors and visual shifts. Symbols as in *A*. *D*: cross-correlation function $\rho_{ep}(\Delta t)$ between reach errors and feedback shifts, along with the Monte Carlo model predictions. Symbols as in *B*. *E*: sensitivity analysis: how predicted cross-correlation functions depend on model parameters. Gray band (data) and green line (M_v model predictions) are the same as those in *B*. Other colored lines represent the cross-correlations predicted by the best-fit M_v model with selected parameters altered, as indicated by the legends. Only the diagonal elements of the parameter matrices *A* and *B* were varied, whereas in the case of *Q* and *R* the entire matrix was scaled.

RESIDUALS OF ONE-STEP-AHEAD PREDICTIONS. If the one-step-ahead model predictions captured the full dynamics of adaptation, then the residual errors should have no statistical structure, i.e., they should be white noise. This can be assessed by the portmanteau test for serial autocorrelations. If significant correlations existed in the model prediction residuals, then the model would be insufficient to account for the dynamics of adaptation and the model would be rejected. For all subjects, the one-step-ahead predictions of both the M_v and the M_p model leave no significant residual correlations in a cross-validation test for the STOCH-P trial blocks (portmanteau test, $P > 0.05$, max. lag $m = 8$).

These results suggest that the LDS models are sufficient to capture the trial-by-trial dynamics of adaptation. However, because the portmanteau test pools all residuals and all time lags into a single statistic, it has relatively low statistical power. This means that more subtle model inaccuracies might not be detectable with this approach. Detecting such inaccuracies is especially important when interpreting the state and output noise terms because model inaccuracies will appear in our model fits as additional noise. Therefore we performed a variety of additional analyses on the model residuals, testing for violations of normality, stationarity, and model linearity. We found no significant evidence for any of these effects, as described in detail in the APPENDIX.

Together, these analyses suggest that the LDS models considered here are indeed sufficient to explain the dynamics of reach adaptation in the STOCH-P trial blocks.

State noise

The two sources of variability in the LDS model—the state noise and the output (or sensorimotor) noise—are conceptually quite different and both will contribute to the overall variability in any measure of performance. Although the output noise is uncorrelated across trials, state noise is accumulated in the state and thus its contribution to the reach variability is correlated across trials. Given that the state noise is often overlooked in models of motor variability, we want to confirm here that the level of state noise is indeed significant.

We use the LRT to compare the M_v or M_p model class to a null hypothesis class with no state noise. In practice, Q cannot vanish entirely or the parameter estimation algorithm would become unstable. Thus for the null hypothesis we use a model with the state noise covariance fixed to a negligible value ($Q = 0.1$ mm^2) relative to the output noise covariance R. The LRT shows that the addition of state noise significantly improves the model fit in the STOCH-P condition for both learning models and for all subjects (M_v: $P < 10^{-4}$; M_p: $P < 0.003$; $n = 10$).

We confirm this result by applying the portmanteau test to the best-fit null hypothesis model (i.e., the best model with $Q = 0.1$ mm^2). These models could not capture the temporal structure of the reach errors: the residuals were significantly correlated across trials (M_v rejected in 10/10 subjects, M_p rejected in 7/10; $P < 0.05$, max. lag $m = 8$). These results establish that state noise contributes significantly to the trial-by-trial sequences of reach error.

Next, we assess the magnitude of the state noise by comparing it to the output noise. As a measure we choose the ratio of the largest eigenvalues of the state and output covariance matrices, v_Q and v_R, respectively, (see also Table 1)

$$k = \sqrt{v_Q / v_R} \tag{9}$$

For all subjects, the two noise terms are on the same order of magnitude, although the output is typically larger by about a factor of two (Fig. 7, open bars). To assess the statistical significance of the ratio k, we compared these values to the 95% confidence values obtained by separately fitting the LDS

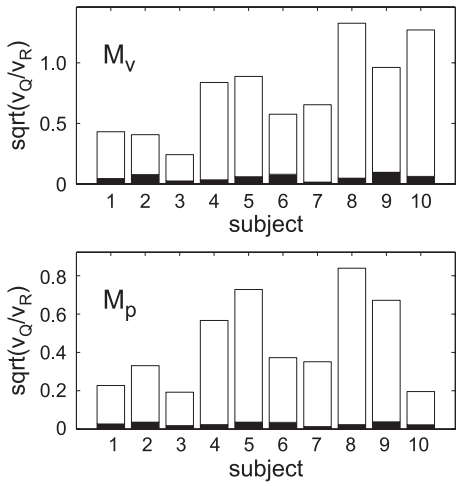

FIG. 7. Magnitude of estimated state noise relative to output noise (open bars) for 2 model classes fit to the STOCH-P data. v_Q and v_R are the largest eigenvalues of the state and output noise covariances, respectively. Filled bars represent the 95% confidence value under the null hypothesis of negligible state noise determined from 1,000 Monte Carlo simulations.

models to each of 1,000 Monte Carlo simulations run with Q reset to 0.1 mm^2 (Fig. 7, filled bars). The k ratios obtained in these simulations are quite small, significantly smaller than the values obtained from the true data. This underscores the conclusion that the state noise is an important feature of the data and not an artifact of the fitting procedure.

Finally, we consider the contribution of state noise to the overall reach error variability. It is not difficult to show that in the case of no visual feedback shift, the LDS models predict an overall reach variance of

$$M_v\text{: Var}(e_t) = R + \sum_{s=0}^{\infty} (A+B)^s Q (A+B)^{s\mathrm{T}} + \sum_{s=0}^{\infty} (A+B)^s BRB^{\mathrm{T}} (A+B)^{s\mathrm{T}}$$

$$M_p\text{: Var}(e_t) = R + \sum_{s=0}^{\infty} A^s Q A^{s\mathrm{T}}$$

We computed the values of these expressions numerically from the best-fit models. We then quantify the fraction of the overall reach variability that is attributed to the output noise (the second term in the equations above), as opposed to the state noise (the first term). For the M_v model there is also a third term corresponding to the effects of feeding the reach error back into the LDS by the input v_t. On average, the estimated contribution of state noise to the overall reach error variability was 23% for the M_p model and 38% for the M_v; error feedback in M_v contributes another 7%. Therefore whereas output noise accounts for more than half of the overall reach endpoint variability, state noise represents a sizable component as well.

Adaptation dynamics generalizes to constant feedback shift

Up to this point we have examined only the adaptation dynamics in the STOCH-P trial blocks. One concern that might arise is that the results we have found, such as the magnitudes of the learning rates and state noise, are specific to the stochastic sequence of feedback shifts. It is important to verify that the conclusions drawn from studies using these dynamical systems techniques will generalize to other experimental paradigms, in particular to the blocked-exposure design traditionally used in studying reach adaptation. Therefore we quantified how well LDS models that were fit to the STOCH-P data predict the results of the CONST-P condition, which is similar to a blocked-exposure design. We focused on predictions of the steady state of adaptation, the statistics of the sequence of reach errors, and the residuals of the one-step-ahead model predictions.

In general, LDS models predict that adaptation should converge to a "steady state" when the input is held constant. However, as a result of the presence of state and output noise, there will be random fluctuations in both the state and the output even after this convergence has occurred. The LDS model predicts both the magnitude of this steady-state reach error and the fluctuations around it. We compared these model predictions to values obtained from the data. The M_v and M_p models make nearly identical predictions for the steady-state error magnitude and these values correlate well with the empirical data across subjects (Fig. 8*A*). There is a small bias, however: the models consistently predict a slightly smaller steady-state error than what is empirically observed (mean bias is 2.7 mm for M_v and 2.8 mm for M_p). Both models make accurate predictions for the SD of the reach error during the steady state (Fig. 8*B*).

Next, we consider how well the M_v and M_p models fit to the STOCH-P data can predict the statistics of the reach errors across the CONST-P trial blocks. Both models provide a good prediction of the variance and autocorrelation of the reach errors as well as the covariance and cross-correlation between the reach errors and the sequence of visual feedback shifts (Fig. 9, *A–D*). This generalization across tasks is not solely attributable to the nature of the CONST-P shift sequence because the model predictions are sensitive to the parameter values (Fig. 9*E*).

Finally, however, we note that the generalization is not perfect. We performed the portmanteau test for serial autocorrelations on the residuals of the one-step-ahead predictors (models fit on STOCH-P data, tested on CONST-P data). For a minority of subjects, the models were unable to fully account for the temporal structure of the reach error sequence (M_v: fits

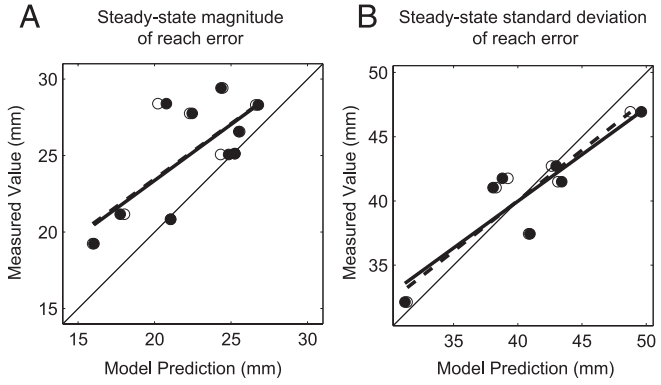

FIG. 8. Comparison of empirical and predicted steady states of adaptation. Predictions were derived from the M_v (●, solid lines) and the M_p (○, dashed lines) models fit to STOCH-P data. Empirical values were averaged over the last 10 trials of each CONST-P trial block. *A*: magnitude of the steady state of adaption with a 30-cm magnitude shift along each axis. Empirical values are averages of the x and y error coordinates. Expression for model predictions is given in Cheng and Sabes (2006). Linear regression of the measured values on the model fits shown in bold lines (M_v: $R^2 = 0.52$, $P = 0.02$; M_p: $R^2 = 0.50$, $P = 0.02$). *B*: SD of the reach error during steady state (σ_e^2 in *Eq. 3a*). Model predictions come from Monte Carlo simulations (see METHODS). Linear regression in bold lines (M_v: $R^2 = 0.79$, $P = 0.007$; M_p: $R^2 = 0.81$, $P = 0.006$).

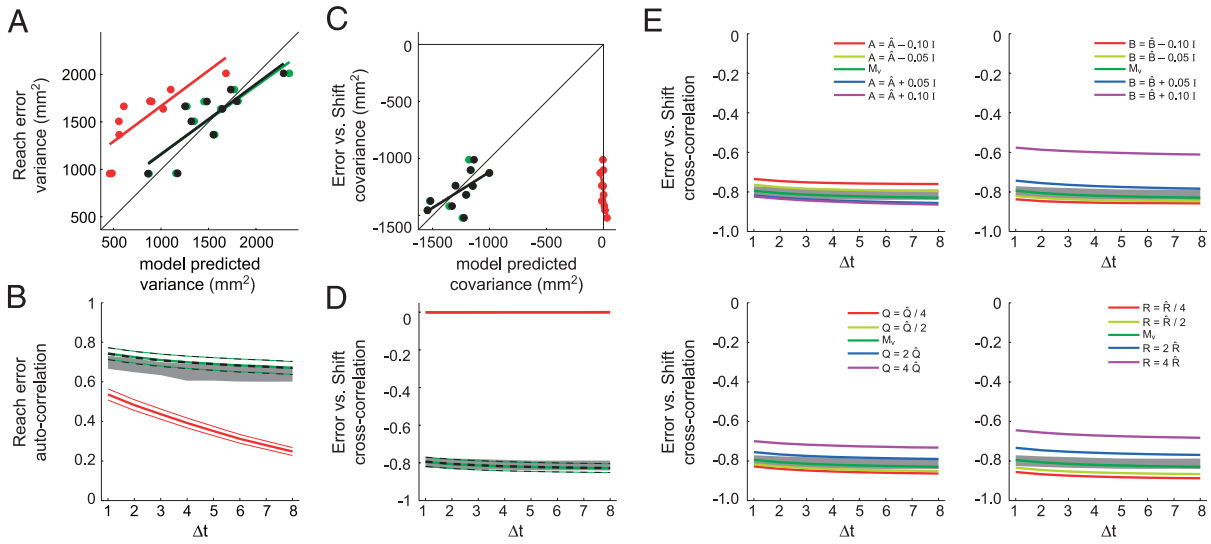

FIG. 9. Dynamics model identified from STOCH-P data can also account for adaptation to constant visual shift. Plotting convention is the same as in Fig. 6. *A*: reach errors variance vs. Monte Carlo model predictions. *B*: autocorrelation function of reach errors for time differences of 1–8 trials and Monte Carlo model predictions. *C*: covariance between reach errors and feedback shifts for individual subjects vs. Monte Carlo model predictions. Linear regression of subject data on model prediction was marginally significant: $P = 0.06$ for the M_v model (green circles and green regression line) and $P = 0.07$ for the M_p model (black circles, thick black regression line). *D*: cross-correlation function between reach errors and feedback shifts for time differences of 1–8 trials, along with the Monte Carlo model predictions. *E*: sensitivity analysis of how predicted cross-correlation functions depend on model parameters.

for 4/10 subjects rejected; M_p: 2/10 rejected; $P < 0.05$ and max. lag $m = 8$).

Taken together these comparisons suggest that the dynamics of adaptation largely generalizes from a stochastic sequence of visual shifts to a constant shift paradigm. Furthermore, the LDS model fit to the stochastic shift data is able to quantitatively predict the key features of the of the blocked-exposure paradigm.

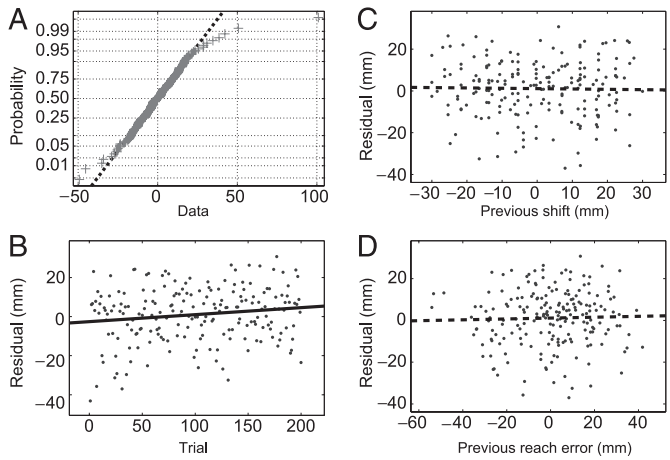

FIG. 10. Examples of statistical analyses performed on the model prediction errors. *A*: normal probability plot for the only residual component (*x*-component, Subject 8) that showed significant deviations from normality ($N = 199$, Lilliefors test, $P = 0.04$). Data-points are represented by crosses; Gaussian data fall on a straight line. Without the single large outlier (*top right* of graph), the deviation from the Gaussian distribution is not significant ($P > 0.2$). *B*: example of significant nonstationary (linear regression, F-test, $P = 0.036$) in the model-fit residual (*y*-component, Subject 1). *C, D*: example plots of model-fit residual (*y*-component, Subject 1) vs. visual shift on the prior trial (*C*) or reach error on the prior trial (*D*). Linear regression shows no significant effect in either plot (F-test, $P = 0.79$ and $P = 0.69$) and no clear nonlinear relationships are discernible.

DISCUSSION

We have shown that the trial-by-trial dynamics of reach adaptation to shifted visual feedback is well described by a simple linear dynamical system. In this model, there are two forces driving changes in the state of adaptation. First, learning is driven by error-corrective feedback, with the state of the system correcting for ≥20% of the error observed in the preceding movement, on average. The data presented here are consistent with two candidate error signals: the visually perceived reach error and the artificial visual shift. Second, adaptation is driven by the internal dynamics of learning, including a decay back to a baseline state and the accumulation of an internal "learning" or state noise. Finally, the LDS model generalizes from the case of stochastic feedback shifts to the more traditional case of constant feedback shifts.

Sufficiency and generalization of the LDS model

One finding of this study is that simple LDS models are sufficient to describe the dynamics of adaptation. If our model captured all the temporal structure in the data, the model prediction residuals should be a white-noise sequence. We therefore analyzed the correlations among and between residuals and various key task variables. We found no significant evidence for autocorrelations in the model residuals, nonstationarity and nonlinearities in the dynamics, or non-Gaussian noise.

Nevertheless, another indication that the LDS models are indeed capturing the dynamics of adaptation is the fact that the models generalize from stochastic to constant feedback shifts. Although the bulk of our analyses support this conclusions, there are three deviations from the model predictions that should be considered. First, the predicted covariances between reach errors and feedback shift were systematically smaller than the empirical values (Fig. 6*C*). Second, the models predicted a slightly smaller steady-state adaptation in the CONST-P

condition (Fig. 8*A*). Third, the portmanteau test for generalization to the CONST-P case failed for a minority of the subjects.

All three of these observations could be explained by an underestimate of about 10 to 20% in the magnitude of the learning rate *B*. The learning rate controls how much the external input affects the state of adaptation and so a more negative *B* would increase the covariance between reach error and feedback shift in the STOCH-P condition. In addition, the magnitude of the steady-state error in the CONST-P condition depends only on the decay parameter *A* and the learning rate *B*. Increasing the magnitude of either parameter would lead to a larger predicted steady state (Cheng and Sabes 2006). Similarly, if the estimated magnitude of *B* is low, there will be a persistent bias in the one-step-ahead prediction of the reach error in the CONST-P trial blocks, resulting in a significant correlation in the prediction residuals across trials. This would explain the occasional failure of the portmanteau test for generalization to the CONST-P condition. Visual inspection confirms that predictions of CONST-P reach errors are indeed biased in the very cases for which the portmanteau test failed (data not shown). Finally, a higher learning rate (more negative *B*) would not significantly degrade the predictions of the cross-correlations between reach errors and feedback shifts (Figs. 6*E* and 9*E*).

Why might the learning rate *B* have been underestimated? One obvious reason would be a bias in the maximum-likelihood–fitting procedure. However, we found no evidence for such a bias in control analyses in which we estimated the LDS parameters from artificial data generated from a known LDS (data not shown). Another possibility is that adaptation is a higher-order system—i.e., subjects maintain a memory of more than just the immediately preceding input—and these older error signals also influence learning. To address this possibility, we fit the stochastic shift data with augmented models in which learning is driven by the two preceding inputs. This model yielded a significant improvement for some subjects (LRT, M_v 2/10 subjects, M_p 6/10, with $P < 0.05$). Because both the feedback shift and the visually perceived error had sizable autocorrelations at a lag of one trial, this analysis had limited power. Therefore it is plausible that such second-order effects are present in all of our data sets. This extra source of input would explain the prediction errors described here, even in the absence of a fitting bias.

A second explanation for imperfect generalization to the constant-shift data could be the presence of multiple timescales of reach adaptation (Smith et al. 2006). Suppose that there were two state variables that contribute to the trial-by-trial task performance: one that learns on the fast timescales described above and one with a much slower learning rate. The effects of the slow-learning system would not be apparent when the visual feedback shift changes on a trial-by-trial basis because its effects would average out across trials. However, when a constant feedback shift is used, the slow learning system would contribute to the state of adaptation. This contribution could account for the discrepancies we observed between the constant shift data and the model predictions.

State noise

We have found that state noise accounts for at least a quarter of the overall trial-by-trial variability in reaching, after discounting the changes arising from our artificial feedback shifts. The presence of significant state noise implies that sensorimotor calibration is changing continually, even without exogenous driving inputs. This model offers a strong counterpoint to the traditional view of motor variability as arising largely from limitations in the sensory and motor peripheries (Donchin et al. 2003; Gordon et al. 1994; Harris and Wolpert 1998; Messier and Kalaska 1990; Osborne et al. 2005; Thoroughman and Shadmehr 2000; van Beers et al. 1998). Neglecting the presence of such state noise in studies of sensorimotor variability can lead to overestimates of those variances. Also, because state noise leads to correlations in movement variability across trials, the application of statistical models that assume independent noise across trials (e.g., Donchin et al. 2003; Thoroughman and Shadmehr 2000) may lead to incorrect conclusions (Cheng and Sabes 2006).

There are several potential sources for the state noise we observed: variability could arise in the sensory processing of the error feedback signals; variability could be injected into the state during the process of adaptation, i.e., as a by-product of the computations that underlie learning; or variability can be introduced in the memory or maintenance of the state across trials. In fact, it is likely that at least some of the state noise comes from each of these sources. Quantifying the relative importance of sources of variability is a direction for further research.

An alternative explanation for the apparent state noise is that our LDS models are deficient in some respect. The resulting error in the state update would then be subsumed into the state noise when estimating the LDS parameters. In the APPENDIX, we argue that the state noise is unlikely to be the result of nonlinearity, nonstationarity, or nonnormal noise in the true process of adaptation. Of course, those analyses would be unable to detect high-order nonlinearity or rapid nonstationarity. As an extreme example, consider the case where the neural circuit that underlies adaptation is made up of a large number of deterministic, nonlinear "units" that combine to approximate a linear learning rule. This circuit is deterministic, but there will be many small fluctuations about the linear learning rule. Although such variability may in fact be "deterministic," from a practical perspective we may view it as "noise."

Another model assumption that could potentially be incorrect is that there is a single process giving rise to the adaptation we study here. We tested whether multiple processes with different timescales (Smith et al. 2006) could account for the state noise. In fact, when we fit the data with a two-timescale model, the state noise was still significant for all subjects (likelihood ratio test). Furthermore, despite having many extra model parameters, the best-fit state noise in the two-timescale model was appreciably lower in only three subjects (data not shown) and, even in those cases, the state noise covariance was within the range of values found for other subjects with the single-timescale model. We conclude that the existence of multiple timescales could not account for the state noise that we observed.

The LDS models would also be deficient if they were missing a significant input signal. Two candidate signals come easily to mind. One candidate is the error feedback from earlier trials, as discussed earlier. However, the estimated state noise is qualitatively unchanged when these earlier inputs are included in the model (data not shown). Another variable that we

did not include in our models is the actual position of the reach target, which was drawn uniformly from a 4-cm square for each trial. However, adding the target position improved the M_p model fit in only two subjects (LRT, $\alpha = 0.05$) and lowered the estimated state noise covariance only marginally.

Finally, we recall that the distinguishing difference between state and output noise in the LDS model is the fact that the state noise creates variability, which is correlated across trials (a random walk), whereas the output noise in uncorrelated (white noise). Therefore noise in the sensory or motor periphery would mimic state noise if it were correlated across trials (on the order of tens of seconds to minutes). Although we know of no evidence for such correlations, they might exist and could account for some fraction of our observed state noise.

Error-driven learning

One clear result from this study is that the trial-by-trial dynamics of reach adaptation are well modeled by an error-corrective learning rule. Furthermore, the rate of learning is quite rapid, with an average correction in the state of $\geq$20% of the last error after each movement. These rapid adaptation dynamics appear to be inconsistent with slower models of learning, such as those based on Hebbian learning rules (Hua and Houk 1997; Salinas and Abbott 1995).

What is less clear, however, is the specific sensory signal that drives learning. We have shown that the visually perceived error and the artificial feedback shift provide equally good explanations of the trial-by-trial changes in reach performance. Indeed, the two models classes corresponding to these input signals are largely equivalent with respect to the present data set (see *Eq. 8*). From a biological perspective, however, these input signals are quite distinct. Determining the feedback shift, for example, requires a comparison between visual and other sensory modalities, whereas the visually perceived error can be computed entirely from retinal signals. Thus it should be possible to design experiments using the LDS modeling approach that better distinguish between these feedback signals. For example, by using small, undetectable jumps in the target position (Magescas and Prablanc 2006), one can dissociate the visually perceived error from a shift in visual feedback.

The LDS model and the mechanisms of adaptation

We have shown that the LDS model provides a concise and accurate description of the trial-by-trial dynamics of reaching. However, we do not believe that this simple class of models can capture the full complexity of sensorimotor adaptation. For example, it is well recognized that there are multiple components of prism adaptation (Harris 1963; Redding and Wallace 1988; Redding et al. 2005; Welch et al. 1974) and evidence for multiple learning and decay rates exists as well (Choe and Welch 1974; Hatada et al. 2006; Smith et al. 2006; Taub and Goldberg 1973). Furthermore, multiple brain areas have been implicated in the process of prism adaptation (Baizer and Glickstein 1974; Baizer et al. 1999; Clower et al. 1996; Kurata and Hoshi 1999). Rather, we see these models as a powerful analytic tool for quantitatively characterizing the dynamics of adaptation in the face of artificial sensorimotor perturbations, the natural and ongoing processes of sensorimotor calibration, and the relationship between these processes. For example, some parameters, such as the state decay, showed little variance across subjects, whereas others, such as the learning rate, showed more variability. Understanding the forces that shape these parameter values over both the short term (i.e., arising from the details of the experimental conditions) and the long term would provide valuable insight into the general mechanisms for the maintenance of accurate sensorimotor control. Finally, the tools developed here can be used not only to relate sensory feedback signals to behavior, but also to relate these psychophysical variables to the underlying patterns of neural activity.

APPENDIX

Analysis of model prediction errors

In this APPENDIX, we test for subtle inaccuracies in the best-fit models with a range of statistical tests on the one-step-ahead prediction residuals. Specifically, we ask whether the residuals are normally distributed and whether there is evidence for nonstationarity or nonlinearity in the true dynamics of learning.

NON-GAUSSIAN NOISE. The LDS models used herein assume that both the state noise q_t and output noise r_t have Gaussian distributions. Under this model, the one-step-ahead prediction errors should also be Gaussian. Deviations from normality in these prediction errors could arise in two ways: the true underlying noise processes could be non-Gaussian, or there could be inaccuracies in the model of learning dynamics. For example, if there were nonlinearities or nonstationarities in the true dynamics of learning, or if we had neglected to include an important additional input signal, then we would not necessarily expect the model residuals to look Gaussian. Therefore we performed a test of normality on the model prediction residuals. Because subjects performed reaches in a two-dimensional environment, the residuals are two-component vectors. Here, and in subsequent tests, we tested each component separately for a total of 20 tests (10 subjects $\times$ 2 components). Of these 20 tests, only one showed a significant deviation from Gaussianity (Lilliefors test, $\alpha = 0.05$). Even this deviation was the result of only a single outlier point (Fig. 10*A*); without the outlier the residual component was not significantly non-Gaussian ($P > 0.2$). Except for the outlier point, the normal probability plot shown in Fig. 10*A* is typical of that observed for other subjects. We conclude that the model residuals are normally distributed.

NONSTATIONARITY. If the true learning dynamics were nonstationary, then we would expect our stationary LDS models to fit better at some times during the experiment and worse at other times. Therefore we plotted the residuals as a function of trial number and looked for changes across trials. Out of 20 such plots, three showed a significant linear dependency of residual on trial number (linear regression, F-test, $\alpha = 0.05$). An example of a significant effect is shown in Fig. 10*B*. Although these effects were observed slightly more often than expected by chance (3/20 = 15%), the significant comparisons had weak correlations ($r^2 < 0.034$) and were never found in both residual components of the same subject. Across subjects there are no discernible nonlinear trends in the residuals, nor were there any apparent changes in the variance of the residuals across trials.

NONLINEARITY. If the true learning dynamics were nonlinear, then the LDS prediction errors would contain a component that was a deterministic function of one of the key variables driving learning. Therefore we examined whether the model-fit residuals across trials covary with either of the key variables that influence the dynamics of learning, the visual shift, and the reach error from the previous trial. Not one of the 20 comparisons showed a significant linear dependency of residual on either the previous visual shift or the previous reach error (linear regression, F-test, $\alpha = 0.05$). Representative examples

are shown in Fig. 10*C* and *D*. As in these examples, there were also no discernible nonlinear relationships between the residuals and the task variables.

GRANTS

This work was supported by the Swartz Foundation, the Alfred P. Sloan Foundation, the McKnight Endowment Fund for Neuroscience, Whitehall Foundation Grant 2004-08-81-APL, and National Eye Institute Grant R01 EY-015679.

REFERENCES

Anderson BDO, Moore JB. *Optimal Filtering*. Englewood Cliffs, NJ: Prentice-Hall, 1979.

Atkeson CG, Hollerbach JM. Kinematic features of unrestrained vertical arm movements. *J Neurosci* 5: 2318–2330, 1985.

Baddeley RJ, Ingram HA, Miall RC. System identification applied to a visuomotor task: near-optimal human performance in a noisy changing task. *J Neurosci* 23: 3066–3075, 2003.

Baizer JS, Glickstein M. Proceedings: role of cerebellum in prism adaptation. *J Physiol* 236: 34P–35P, 1974.

Baizer JS, Kralj-Hans I, Glickstein M. Cerebellar lesions and prism adaptation in macaque monkeys. *J Neurophysiol* 81: 1960–1965, 1999.

Bedford FL. Perceptual and cognitive spatial learning. *J Exp Psychol* 19: 517–530, 1993.

Cheng S, Sabes PN. Modeling sensorimotor adaptation as linear dynamical system. *Neural Comput* 18: 760–793, 2006.

Choe CS, Welch RB. Variables affecting the intermanual transfer and decay of prism adaptation. *J Exp Psychol* 102: 1076–1084, 1974.

Clower DM, Hoffman JM, Votaw JR, Faber TL, Woods RP, Alexander GE. Role of posterior parietal cortex in the recalibration of visually guided reaching. *Nature* 383: 618–621, 1996.

Davies N, Newbold P. Some power studies of a portmanteau test of time-series model specification. *Biometrika* 66: 153–155, 1979.

Donchin O, Francis JT, Shadmehr R. Quantifying generalization from trial-by-trial behavior of adaptive systems that learn with basis functions: theory and experiments in human motor control. *J Neurosci* 23: 9032–9045, 2003.

Ghahramani Z, Hinton GE. Parameter estimation for linear dynamical systems. Technical Report CRG-TR-96-2. Toronto, Canada: Univ. of Toronto, 1996.

Gordon J, Ghilardi M, Ghez C. Accuracy of planar reaching movements. I. Independence of direction and extent variability. *Exp Brain Res* 99: 97–111, 1994.

Harris CM, Wolpert DM. Signal-dependent noise determines motor planning. *Nature* 394: 780–784, 1998.

Harris CS. Adaptation to displaced vision: visual, motor, or proprioceptive change? *Science* 140: 812–813, 1963.

Hatada Y, Rossetti Y, Miall RC. Long-lasting aftereffect of a single prism adaptation: shifts in vision and proprioception are independent. *Exp Brain Res* 173: 415–424, 2006.

Hay JC, Pick HL. Visual and proprioceptive adaptation to optical displacement of the visual stimulus. *J Exp Psychol* 71: 150–158, 1966.

Held R, Gottlieb N. Technique for studying adaptation to disarranged hand-eye coordination. *Percept Mot Skills* 8: 83–86, 1958.

Hosking JRM. The multivariate portmanteau statistic. *J Am Stat Assoc* 75: 602–608, 1980.

Hua SE, Houk JC. Cerebellar guidance of premotor network development and sensorimotor learning. *Learn Mem* 4: 63–76, 1997.

Kurata K, Hoshi E. Reacquisition deficits in prism adaptation after muscimol microinjection into the ventral premotor cortex of monkeys. *J Neurophysiol* 81: 1927–1938, 1999.

Ljung L. *System Identification: Theory for the User* (2nd ed.). Upper Saddle River, NJ: Prentice Hall, 1999.

Magescas F, Prablanc C. Automatic drive of limb motor plasticity. *J Cogn Neurosci* 18: 75–83, 2006.

Messier J, Kalaska JF. Differential effect of task conditions on errors of direction and extent of reaching movement. *Exp Brain Res* 125: 139–152, 1990.

Miles F, Fuller J. Adaptive plasticity in the vestibulo-ocular responses of the rhesus monkey. *Brain Res* 80: 512–516, 1974.

Nemenman I. Fluctuation-dissipation theorem and models of learning. *Neural Comput* 17: 2006–2033, 2005.

Optican LM, Robinson DA. Cerebellar-dependent adaptive control of primate saccadic system. *J Neurophysiol* 44: 1058–1076, 1980.

Osborne LC, Lisberger SG, Bialek W. A sensory source for motor variation. *Nature* 437: 412–416, 2005.

Redding G, Wallace B. Adaptive mechanisms in perceptual-motor coordination: components of prism adaptation. *J Mot Behav* 20: 242–254, 1988.

Redding GM, Rossetti Y, Wallace B. Applications of prism adaptation: a tutorial in theory and method. *Neurosci Biobehav Rev* 29: 431–444, 2005.

Salinas E, Abbott LF. Transfer of coded information from sensory to motor networks. *J Neurosci* 15: 6461–6474, 1995.

Scheidt R, Dingwell J, Mussa-Ivaldi F. Learning to move amid uncertainty. *J Neurophysiol* 86: 971–985, 2001.

Shumway RH, Stoffer DS. An approach to time series smoothing and forecasting using the EM algorithm. *J Time Series Anal* 3: 253–264, 1982.

Smith MA, Ghazizadeh A, Shadmehr R. Interacting adaptive processes with different timescales underlie short-term motor learning. *PLoS Biol* 4: e179, 2006.

Sober S, Sabes P. Flexible strategies for sensory integration during motor planning. *Nat Neurosci* 8: 490–497, 2005.

Stuart A, Ord JK. *Kendall's Advanced Theory of Statistics* (5th ed). New York: Oxford Univ. Press, 1987.

Taub E, Goldberg L. Prism adaptation: control of intermanual transfer by distribution of practice. *Science* 180: 755–757, 1973.

Thoroughman KA, Shadmehr R. Learning of action through adaptive combination of motor primitives. *Nature* 407: 742–747, 2000.

van Beers R, Sittig A, Denier van der Gon J. The precision of proprioceptive position sense. *Exp Brain Res* 122: 367–377, 1998.

Welch RB. *Perceptual Modification: Adapting to Altered Sensory Environments*. New York: Academic Press, 1978.

Welch RB, Choe CS, Heinrich DR. Evidence for a three-component model of prism adaptation. *J Exp Psychol* 103: 700–705, 1974.